Upper limits of HO2 in the atmosphere of Mars from the ExoMars Trace Gas Orbiter

Juan Alday, Alexander Trokhimovskiy, Denis A Belyaev, Anna A Fedorova, James A Holmes, Manish R Patel, Jonathon P Mason, Franck Lefèvre, Kevin S Olsen, Franck Montmessin, et al.

Monthly Notices of the ROYAL ASTRONOMICAL SOCIETY

MNRAS **532,** 4429–4435 (2024) https://doi.org/10.1093/mnras/stae1814
Advance Access publication 2024 July 26

Upper limits of HO_2 in the atmosphere of Mars from the ExoMars Trace Gas Orbiter

Juan Alday ,[1]★ Alexander Trokhimovskiy,[2] Denis A. Belyaev,[2] Anna A. Fedorova,[2] James A. Holmes,[1] Manish R. Patel,[1] Jonathon P. Mason,[1] Franck Lefèvre,[3] Kevin S. Olsen,[4] Franck Montmessin,[3] Oleg Korablev,[2] Lucio Baggio[3] and Andrey Patrakeev[2]

[1]*School of Physical Sciences, The Open University, Milton Keynes MK7 6AA, UK*
[2]*Space Research Institute (IKI), Moscow 117997, Russia*
[3]*LATMOS, Guyancourt 78280, France*
[4]*AOPP, University of Oxford, Oxford OX1 3PU, UK*

Accepted 2024 July 18. Received 2024 July 16; in original form 2024 May 13

ABSTRACT

Odd-hydrogen (HO_x) species have a crucial role in regulating the chemistry of the atmosphere of Mars and are important to understand some of the most fundamental aspects regarding its atmospheric composition such as the long-term stability of CO_2. Despite the key role of these species for our understanding of the Martian photochemistry, there is little observational evidence constraining their abundances. In this study, we use infrared solar occultation observations from the Atmospheric Chemistry Suite aboard the ExoMars Trace Gas Orbiter to search for spectral signatures of HO_2 in the atmosphere of Mars. In our analysis of the data, we retrieve vertical profiles of pressure, temperature, and water vapour mixing ratio, but are unable to confidently detect the presence of HO_2 features in the spectra. We report upper limits of 15 ppbv (5σ), which represents an order of magnitude improvement with respect to previous investigations. Comparing the derived upper limits with the expectations from 3-dimensional Global Climate Models, we find that approximately an order of magnitude improvement in the instrument sensitivity would be required to detect this molecule and/or constrain the models.

Key words: radiative transfer – planets and satellites: atmospheres – planets and satellites: terrestrial planets.

1 INTRODUCTION

Odd-hydrogen (HO_x) species such as OH and HO_2 have a crucial role in regulating the chemistry of the atmosphere of Mars. This role was first evidenced by the slow recombination rate of the photolysis products of CO_2 (i.e. CO + O), which required a catalytic pathway to maintain a 95 per cent CO_2 atmosphere on Mars. McElroy & Donahue (1972) and Parkinson & Hunten (1972) demonstrated that the stability of CO_2 in the Martian atmosphere holds due to reactions of its photolysis products with HO_x ($CO + OH \rightarrow CO_2 + H$), evidencing the importance of these photochemical species in shaping the composition of the Martian atmosphere.

Despite the key role these species have regulating the Martian atmospheric chemistry, there is little observational evidence constraining their abundances. The abundance of HO_2 on Mars has never been determined, and the most constraining measurements made using ground-based spectroscopy revealed a 3σ upper limit of approximately 200 ppbv (Villanueva et al. 2013). In the case of OH, its presence was first detected as a night glow between 40–60 km in the polar winter atmosphere using infrared measurements from the Compact Reconnaissance Imaging Spectrometer for Mars (CRISM) aboard Mars Reconnaisance Orbiter (MRO) (Clancy et al. 2013). However, while these measurements correspond to the first detection of OH in the atmosphere of Mars, the observed emission originates from excited OH molecules produced in specific photochemical reactions, not allowing a derivation of the total density of OH in the atmosphere of Mars. Recently, OH fluorescent emissions were detected using ultraviolet measurements from the Imaging Ultraviolet Spectrograph (IUVS) aboard the Mars Atmosphere and Volatile EvolutioN (MAVEN) mission, which allow the direct retrieval of the density of OH (Stevens et al. 2024). However, these measurements are restricted to the upper atmosphere, only allowing the retrieval of the OH densities above 110 km, where the OH emissions can effectively be separated from the underlying solar scattered component.

Understanding of the odd-hydrogen chemistry in the atmosphere of Mars is on the other hand often inferred from measurements of the abundances of other species. For instance, photochemical species such as O_3, CO, and H_2O_2 are highly sensitive to the abundance of odd-hydrogen and are often used as tracers of the HO_x chemistry. Current numerical models of the atmosphere of Mars are able to explain the general seasonal and latitudinal patterns of these measured chemical tracers (Lefèvre 2004; Holmes et al. 2018; Daerden et al. 2019). However, the models tend to underestimate the absolute abundances of O_3 and CO in the atmosphere, suggesting that the representation of HO_x oxidation is too efficient. Implementation of additional processes such as the uptake of HO_x on water ice clouds

★ E-mail: juan.alday@open.ac.uk

in 3D global climate models (GCMs), as well as in 1D models, led to an improvement in the model/measurement comparisons in some particular seasons and locations (Lefèvre et al. 2008, 2021; Brown et al. 2022), but there is a large uncertainty on the role of these processes in affecting the chemistry of the Martian atmosphere (Daerden et al. 2023).

Direct measurements of HO_x in the atmosphere of Mars could provide crucial information for constraining the role of heterogeneous reactions and determining the oxidation power of the atmosphere of Mars, helping us unravel some of the fundamental gaps in our understanding of the atmospheric chemistry. In this study, we analyse infrared solar occultation measurements made with the Atmospheric Chemistry Suite (ACS) aboard the ExoMars Trace Gas Orbiter (TGO) to search for spectral signatures of HO_2 and constrain its abundance in the atmosphere of Mars. In Section 2, we provide a description of the ACS measurements analysed in this study. Section 3 summarizes the radiative transfer analysis of the data, and the main results of our search are presented in Section 4. Finally, Section 5 summarizes the main conclusions of this study.

2 ACS MEASUREMENTS

In this study, we use measurements from the mid-infrared (MIR) channel of ACS. ACS MIR is an echelle cross-dispersion spectrometer designed to perform infrared observations of the Martian atmosphere in a spectral range between 2.3–4.2 μm at a high spectral resolution ($\lambda/\Delta\lambda\sim$ 30 000) (Korablev et al. 2018). To attain high spectral resolution across the entire spectral range, ACS MIR incorporates a secondary movable grating that enables the selection of 7–25 diffraction orders based on the tilt of the grating. This secondary grating can take up to ten positions, allowing the acquisition of a relatively large simultaneous spectral range across the 2.3–4.2 μm range.

Here, we analyse measurements made with secondary grating position #13, which allows the selection of 25 diffraction orders (191–215) covering a spectral range between 3200–3625 cm^{-1}. This range includes absorption features from several gaseous species such as CO_2, H_2O, as well as several trace species previously undetected in the atmosphere of Mars. In addition, this spectral range includes a feature of water ice that allows the simultaneous retrievals of cloud optical depth and particle size distribution. The ACS MIR data from secondary grating position #13 was recently used to derive upper limits for the relative abundances of NH_3, HCN, and HC_3N (Trokhimovskiy et al. 2024).

The ACS MIR spectrometer operates in the so-called solar occultation mode, in which measurements of the Sun are continuously performed as the TGO moves along its orbit. During the ingresses and egresses, the instrument's line-of-sight crosses the atmosphere through the limb of the planet, with the relative tangent altitude of the Sun above the Martian surface varying throughout the observation until it finally disappears behind the Mars disc. The uppermost altitudes are used to define the reference solar spectrum, which is then used to generate the transmission spectra at the altitudes below. On the other end, the observations at the lowermost altitudes, where the Sun is concealed by the Mars disc, are used to refine the calibration of the observations (see fig. 1 in Alday et al. 2021b for a detailed description of the geometry of the observations). This observation strategy allows us to generate transmission spectra at different tangent altitudes above the Mars surface and study the vertical distribution of different atmospheric properties.

In each of the occultation opportunities by ACS MIR, one of the ten secondary grating positions is selected. The choice of positions is made to maximize the instrument's science return, and the strategy has varied throughout the mission. In the case of secondary grating position #13, used in this study, it has been intermittently utilized throughout the mission operations using different measuring commands. Here, we analyse the secondary grating position #13 observations made using a dedicated pointing that allows an effective separation of the diffraction orders on the detector frame, and an increased integration time of 9 ms that improves the signal-to-noise ratio of the spectra. With these constraints, we report the analysis of 200 observations from April 2022 to May 2023, which corresponds to solar longitude $L_S = 212^\circ$ in Martian Year (MY) 36 to $L_S = 63^\circ$ in MY37.

3 RADIATIVE TRANSFER ANALYSIS

The radiative transfer analysis of the ACS MIR solar occultation spectra is performed using the NEMESIS radiative transfer algorithm (Irwin et al. 2008), which has been previously used for the characterisation of several different atmospheric parameters in the atmosphere of Mars with this instrument (e.g. Alday et al. 2021a, 2023). In our scheme, all gaseous absorption is modelled using pre-tabulated look-up tables calculated using the 2020 edition of the HITRAN data base (Gordon et al. 2022). The calculations of the absorption cross-sections of water vapour account for the pressure broadening coefficients relevant for CO_2-dominated atmospheres (Gamache, Farese & Renaud 2016; Devi et al. 2017; Régalia et al. 2019). In the case of the rest of the gases retrieved in this analysis (i.e. CO_2 and HO_2), the pressure broadening coefficients are calculated using the standard parameters tabulated in the HITRAN data base.

Our analysis of the ACS MIR spectra starts with the selection of several spectral windows to retrieve the atmospheric pressure and temperature, as well as the gaseous abundances of H_2O and HO_2. For the retrieval of the pressure and temperature profiles, we select a spectral window between 3490–3499 cm^{-1} in diffraction order 208, which allows us to retrieve these parameters up to an altitude of approximately 100 km (see Fig. 1). The retrieval of water vapour is performed in two spectral windows (3442–3450 cm^{-1} and 3520–3530 cm^{-1}) in diffraction orders 205 and 210, respectively (see Fig. 1). Due to the highly variable nature of the water vapour density in the atmosphere of Mars, the uppermost altitudes at which its spectral signatures can be detected in these spectral windows are also variable, but they can reach altitudes of approximately 90 km during the perihelion season. Finally, the spectral signatures of HO_2 are searched for in a spectral window between 3410–3419 cm^{-1} in diffraction order 203. We find this window to be particularly suitable for the search of HO_2 within the measured spectral range because while the strength of this absorption feature is among the strongest together with those at 3455 and 3526 cm^{-1} in diffraction orders 206 and 210, the contamination from overlapping CO_2 features is minimized with respect to the two other absorption features.

After the data within the desired spectral windows has been selected, we perform a pre-processing of the spectra in order to refine the wavenumber calibration and calculate the instrument lineshape (ILS). This is performed in a single spectrum within each occultation selected so that the depth of the absorption lines is between 0.05–0.1 in transmission units. This approach, similar to that performed by Belyaev et al. (2021), ensures the selection of absorption lines that are several times larger than the noise level but that are not heavily saturated, which is ideal for the characterisation of the wavenumber calibration and ILS. Once the measured spectrum is selected, we calculate a high spectral resolution spectrum accounting

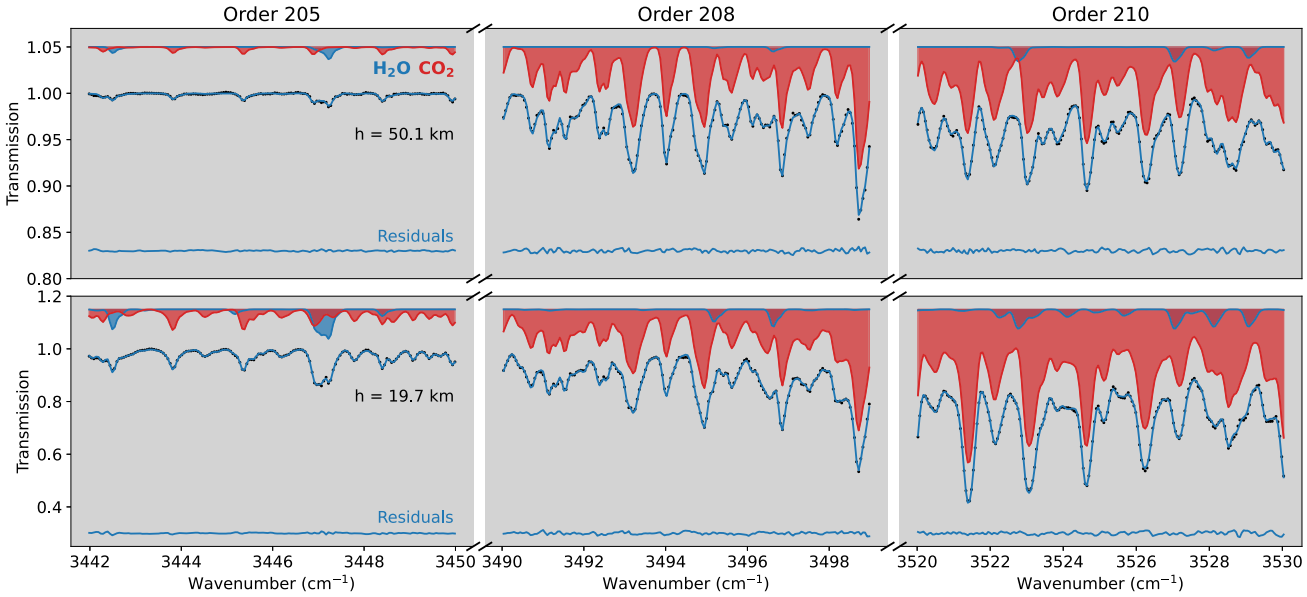

Figure 1. ACS MIR transmission spectra (dots) and best fits to the data (solid lines) measured in orbit 20 006 at 20 (top) and 50 (bottom) km within the spectral windows used to retrieve the vertical profiles of temperature, pressure and water vapour mixing ratio. The residuals between the measured and modelled spectra are also shown in each panel, together with the contribution from each gas to each spectrum, adding a constant offset in both to improve the clarity of the figure.

for the absorption of CO_2 and H_2O using the atmospheric properties from the Mars Climate Data base (Millour et al. 2022). Then, we quantify the refined parameters for the wavenumber calibration and the double Gaussian ILS (Alday et al. 2019) by fitting the high spectral resolution spectrum to the measured one.

Once the characterisation of the spectra has been performed, we carry out the retrievals of the atmospheric parameters, which are separated in two steps. First of all, we perform the retrievals of pressure and temperature from diffraction order 208. Then, the pressure and temperature profiles are fixed, and we retrieve the volume mixing ratios of H_2O and HO_2 from the rest of the spectral windows. In the following sections, we describe in more detail each of these steps.

3.1 Retrievals of pressure, temperature, and water vapour

The retrieval of temperature and pressure is performed using the NEMESIS algorithm following the scheme presented in previous studies using ACS MIR data (e.g. Alday et al. 2021a, 2023). In this scheme, the temperature and pressure is derived from the CO_2 absorption features based on the assumption of a known CO_2 volume mixing ratio and the hydrostatic equilibrium relation. In our state vector, the parameters that are iterated and retrieved are the temperature profile and the pressure at an altitude of approximately 30 km, with the rest of the pressure levels being computed based on the hydrostatic relation. The parameters in the state vector are then varied following the Optimal Estimation formalism (Rodgers 2000; Irwin et al. 2008) until convergence is achieved after approximately five iterations.

After the pressure and temperature profiles have been retrieved, these are fixed, and the retrieval of the water vapour abundance is performed. The first step in our retrieval scheme is essential for the derivation of volume mixing ratios of trace species from the solar occultation spectra, which are otherwise only sensitive to the partial densities of the gases. The retrieval of the water vapour volume mixing ratios is similarly performed using an optimal estimation approach on the spectra from diffraction orders 205 and 210. Once the retrieved water vapour profiles have been obtained from these two spectral windows, we calculate the weighted average profiles following the approach described in Alday et al. (2021b).

Fig. 2 shows the retrieved profiles of temperature and water vapour mixing ratio for the whole data set analysed in this study. Given the repeatable nature of the ground-track of the TGO solar occultations, the variations in our data set may be compared to first order with those derived in other studies in previous MYs (e.g. Belyaev et al. 2021, 2022; Alday et al. 2021a; Aoki et al. 2022; Fedorova et al. 2023). During the second half of MY36, when Mars is close to perihelion, water vapour peaks in the southern hemisphere and can rise to high altitudes thanks to the increased elevation of the hygropause level. During this season, the water vapour abundance between ∼20–40 km in the winter hemisphere (i.e. north) is nevertheless also high due to the enhancement of the water transport from the southern to the northern hemisphere. At the beginning of MY37, with the decrease of the dusty season, the temperatures in the middle atmosphere decrease, and so does the hygropause level, which confines water vapour to low altitudes (<20 km) in the equatorial region. For a detailed description of the climatology of the water vapour vertical distribution from the ExoMars TGO, we refer the readers to the dedicated studies reported in Fedorova et al. (2023) and Aoki et al. (2022).

3.2 Search for spectral signatures of HO_2

The last step of our radiative transfer analysis relates to the search for spectral signatures of HO_2 in the ACS MIR spectra. In this case, we use a modified approach with respect to the retrieval of the water vapour volume mixing ratio because of two main reasons:

(i) The gaseous mixing ratios in the NEMESIS algorithm are carried in logarithmic space, which impedes the retrieval of negative abundances. While this is a realistic approach, enabling the retrieval of negative abundances allows a more thorough statistical analysis

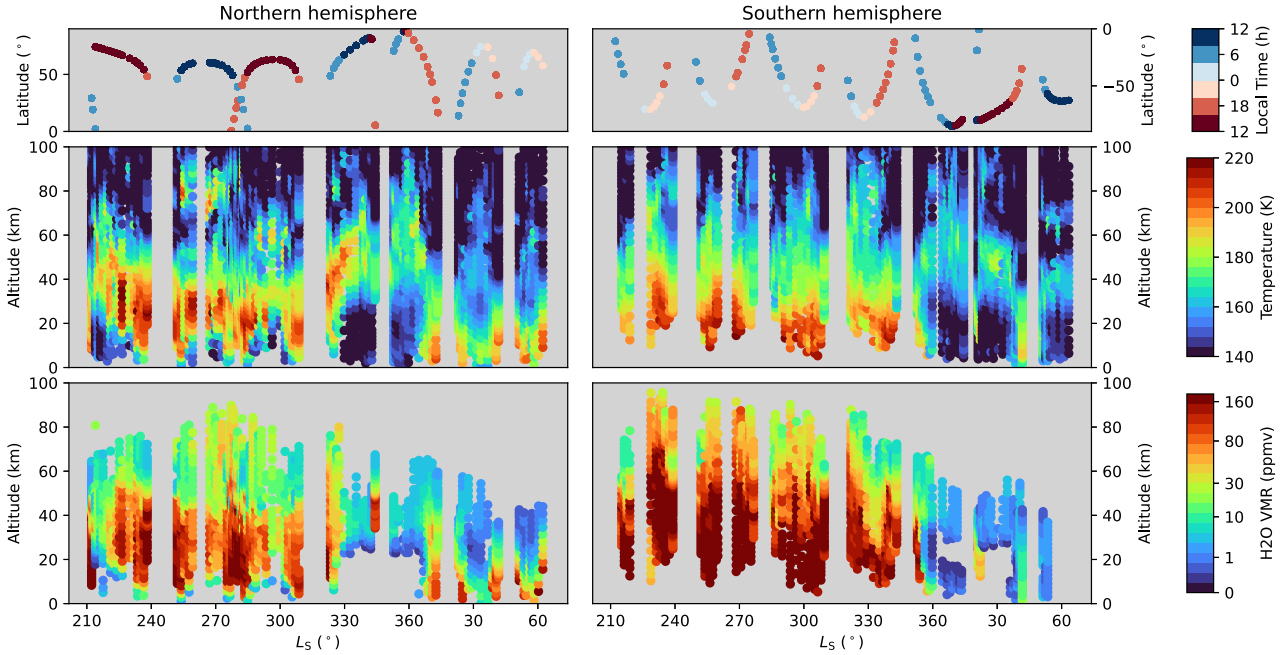

Figure 2. Climatology of temperature and water vapour volume mixing ratio during the second half of MY36 and the beginning of MY37. The top panel shows the evolution of the latitude of the tangent point of the ACS occultations as a function of solar longitude, coloured by the local time of the observation, for the northern (left) and southern (right) hemispheres. The panels below show the retrieved profiles of temperature (middle) and water vapour mixing ratio (bottom) for each of the hemispheres. The water vapour profiles only show the measurements with uncertainties lower than 50 per cent.

of the retrievals in cases where the depth of the spectral features are similar or smaller than the measurement noise.

(ii) The retrieval framework in the NEMESIS algorithm is based on the optimal estimation formalism, which aims to fit the measured spectrum with the forward model with a solution that is closest to the *a priori* state vector (Rodgers 2000). For our purposes, in order to search for the presence of weak spectral signatures in the data, we find it more appropriate to use a non-linear least squares framework that only minimizes the difference between the measured and modelled spectra.

Based on these constraints, we developed a modified approach for the search of spectral signatures of HO_2 in the ACS spectra. In our scheme, each spectrum is analysed independently, fitting the gaseous abundances of CO_2, H_2O, and HO_2, together with a polynomial function to describe the continuum. The gaseous absorption is modelled using the radiative transfer routines in the NEMESIS algorithm, based on the retrieved pressure and temperature profiles retrieved in the previous step (see Section 3.1). However, in this case we fit the parameters using the LMFIT optimisation package, which works following the Levenberg–Marquardt algorithm (Newville et al. 2014).

Since the absorption features of CO_2 and HO_2 partially overlap, we divide our approach into two steps, which are summarized in Fig. 3. First of all, we fit the spectrum by varying the 'background' species CO_2 and H_2O together with the polynomial baseline. Then, the parameters are fixed, and we perform a retrieval of the HO_2 abundance, which in this case is permitted to generate negative values. In each spectrum, the retrieval provides a value for the HO_2 volume mixing ratio together with its associated uncertainty, which are used to define detections or non-detections: if the retrieved volume mixing ratio is five or more times larger than the uncertainty ($\geq 5\sigma$) the retrieval is flagged as a potential detection and subject for visual inspection, while anything below that is flagged as an upper limit.

The sensitivity of the spectra to the abundance of HO_2 at different altitudes follows a similar distribution to that reported in previous searches for trace gas signatures with the TGO occultations (Korablev et al. 2019; Knutsen et al. 2021; Montmessin et al. 2021; Olsen et al. 2021; Braude et al. 2022; Trokhimovskiy et al. 2024). The retrieved uncertainties follow a 'bended knee' variation with altitude (see Fig. 3), arising from the enhanced sensitivity to the gaseous abundances with decreasing altitude due to the increase in the line-of-sight column density, and the decrease of the signal-to-noise ratio due to dust extinction, which peaks in the lowermost observed altitudes. As a result, the optimal sensitivity is found at a certain altitude where the line-of-sight column density is high enough but the signal attenuation by dust is not too strong.

4 ANALYSIS OF THE HO_2 UPPER LIMITS

4.1 Upper limit statistics

The retrieval methodology developed for the search of HO_2 spectral signatures presented in Section 3.2 is applied to all the ACS MIR secondary grating position #13 observations. Fig. 4 presents a summary of the results from our search for HO_2 in the atmosphere of Mars. The left panel on this figure represents the 'Uncertainty Normalized Abundance' (UNA; Knutsen et al. 2021), defined as the ratio between the retrieved HO_2 abundance and its associated uncertainty (UNA $= q/q_{\rm err}$), metric that is used to filter spectra for potential detection of the gas signatures and subject to visual inspection. On the other hand, the right panel shows the 5σ upper limits for the abundance of HO_2 (i.e. $5 \times q_{\rm err}$) derived from our analysis.

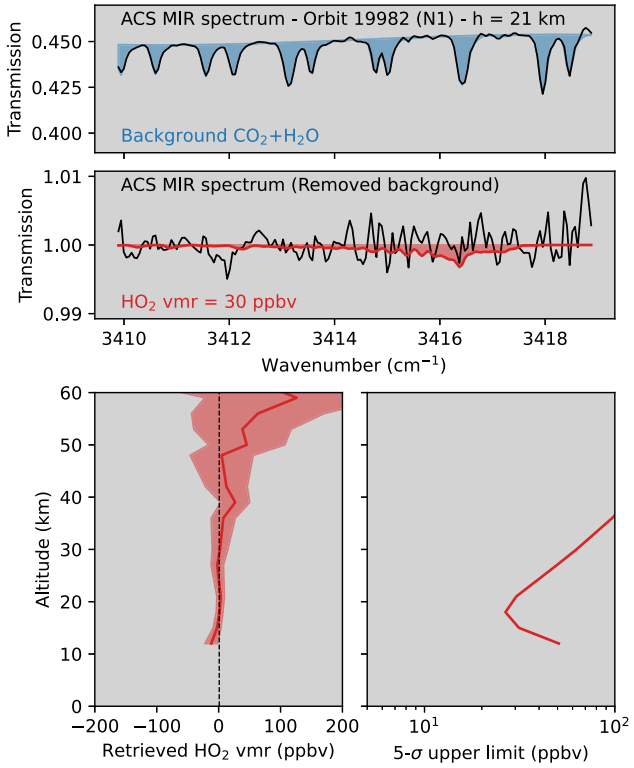

Figure 3. Summary of the methodology to search for the spectral signatures of HO_2. The top panel shows an example of an ACS MIR spectrum (solid line) together with the fitted contributions from CO_2, H_2O and the continuum, which is modelled using a polynomial function (shaded area). In the middle panel, we show the measured spectrum after the previously fitted contributions have been removed (solid line), together with the spectral signature of 30 ppbv of HO_2 (shaded area). The bottom left panel shows the retrieved volume mixing ratio of HO_2 (solid line) for this occultation at different altitudes, as well as the retrieved uncertainty in the HO_2 abundance (shaded area). The bottom right panel shows the derived 5σ upper limit for HO_2.

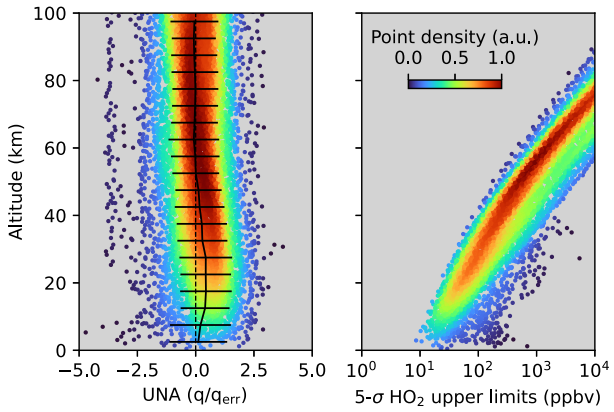

Figure 4. Summary of the HO_2 detection attempts. The points on the left panel show the UNA calculated from each of the spectra, coloured by the density of measurements. The solid black line in this panel shows the averaged UNA at each altitude level, with the errorbars representing the standard deviation of the measurements. The black dashed line represents the zero level. The right panel represents the 5σ upper limits derived from the entire data set analysed in this study, where the colour of the points represents the density of measurements.

From a perspective of the UNA values calculated in each individual spectrum, represented by points in Fig. 4, a detection would be considered when UNA $\geq$ 5. Our retrievals suggest that no spectra reveal detections with UNA $\geq$ 5 and four spectra revealed 3 < UNA < 3.5 in three different occultations. Visual inspection of the fits did not reveal a particularly clear spectral signature of HO_2 in the spectra. In addition, the retrieved volume mixing ratios were large (between 60 ppbv and 800 ppbv) compared with the expectations from the current knowledge of the Martian atmospheric photochemistry (see Section 4.2). Therefore, we conclude that no confident detection of the spectral signature of HO_2 was observed in the ACS MIR spectra analysed in this study.

From a global perspective, the UNA distribution calculated from all measurements should follow a Gaussian function with a standard deviation of one and centered at zero in the absence of detectable trace gas abundances (Knutsen et al. 2021). This expected behaviour in the UNA distribution, represented in Fig. 4 by a black solid line, is what we generally observe in the majority of our retrievals. Our statistics suggest that the standard deviation of the UNA distribution is 1.05, which indicates that the uncertainties from the retrievals are well characterised. In most altitude levels, the UNA distribution is centered on zero, suggesting that no abundance of HO_2 is detectable in a global perspective. Between 10–30 km, the distribution is centered at ∼0.4, which suggests that the retrievals are on average returning positive abundances in this altitude range. However, the statistical significance of this positive mean is small and far from being considered a confident detection of HO_2 in the atmosphere of Mars.

The non-detection of a clear signature of HO_2 in the ACS spectra only allows us to derive upper limits for the abundance of this molecule, which are shown on the right panel of Fig. 4. Our results suggest that the lowest upper limits in our data set occur at approximately 10 km, with values of approximately 15 ppbv (5σ). Above this altitude, the upper limits increase exponentially due to the exponential decrease of the line-of-sight column density with increasing altitude. This value of 15 ppbv represents the lowest upper limit on the abundance of HO_2 to date, which is an improvement of an order of magnitude with respect to previous investigations (∼200 ppbv, Villanueva et al. 2013).

4.2 Comparison with the expectations from OpenMARS

When gases are well mixed in the atmosphere, the lowest upper limits derived from the observations represent the tightest constraints on their abundances. However, in the case of HO_2, given its strong dependency on the highly variable water vapour density (see Fig. 2), its abundance is not expected to be well mixed (Lefèvre & Krasnopolsky 2017). Therefore, while the lowest upper limits of ∼15 ppbv are found at 10–20 km, our observations might be more constraining in some other altitude range. In order to investigate whether our reported upper limits are able to constrain current 3D chemistry models, we compare them with the expectations on the HO_2 abundance from the OpenMARS reanalysis data set (Holmes et al. 2022; Holmes, Lewis & Patel 2024).

OpenMARS is a data set that combines the simulations of a GCM including photochemistry with the assimilation of temperature, water vapour, and dust column information from measurements made by the MRO and the ExoMars TGO to obtain an accurate and global representation of the atmosphere of Mars (Holmes et al. 2022). At the time of writing of this paper, the OpenMARS data base only includes information up to the end of MY35 and therefore does not cover the period of the ACS observations analysed in this study (i.e.

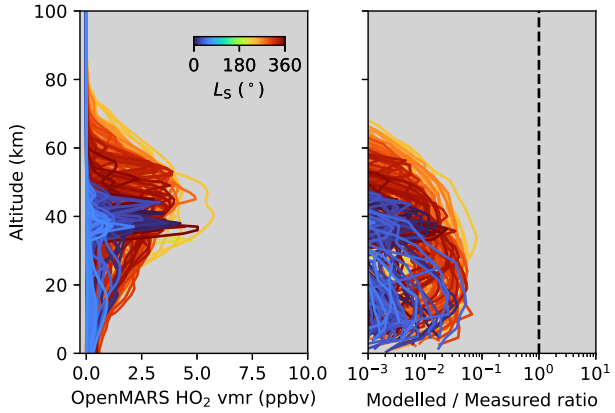

Figure 5. Comparison of the upper limits derived from the ACS MIR spectra with respect to the predictions of the HO_2 abundance from the OpenMARS data set. The left panel shows the simulated HO_2 volume mixing ratios from the OpenMARS data set during MY35 at the locations and times of the ACS MIR occultations during MY36 and MY37, coloured by the solar longitude of the occultation. The right panel shows the ratio between the simulated HO_2 mixing ratios with respect to the 5σ upper limits derived from the ACS occultations.

second half of MY36 and beginning of MY37). Nevertheless, given that none of these years were particularly different in terms of the dust activity (i.e. none of them hosted a Global Dust Storm), we compare our upper limits in MY36 and MY37 with the expectations from OpenMARS during MY35, at the location, solar longitude, and local time of the ACS occultations (see Fig. 5).

The left panel in Fig. 5 shows the simulated vertical profiles of the HO_2 mixing ratio from the OpenMARS data set. During the second half of the year (orange and red profiles), coinciding with the dusty season, the HO_2 mixing ratio is expected to increase with altitude from values of 1–2 ppbv between 0–20 km to 4–5 ppbv at 40–50 km, altitudes at which the volume mixing ratios start decreasing until essentially disappearing above 60–70 km. On the other hand, after the end of the dusty season (blue profiles), when water is confined to the lower layers of the atmosphere, the abundance of HO_2 is expected to be lower than during the dusty season, especially above 20 km. The order of magnitude and variations of the HO_2 abundance in the OpenMARS data set are similar to those reported in other studies (e.g. Lefèvre & Krasnopolsky 2017).

The right panel in Fig. 5 shows the ratio between the simulated abundances of HO_2 and the derived upper limits from the ACS observations. The figure shows that the modelled profiles are always lower in abundance than the upper limits, meaning that the sensitivity of the ACS spectra is not high enough to constrain the chemical models. In particular, a sensitivity of approximately an order of magnitude higher is required to detect HO_2 and/or constrain the chemical models during perihelion, while about two orders of magnitude would be required for monitoring the seasonal and spatial variations of HO_2 in the atmosphere.

5 CONCLUSIONS

Odd-hydrogen species such as OH and HO_2 have a key role regulating the Martian atmospheric photochemistry and they are involved in some of the most fundamental aspects regarding the atmospheric chemistry and composition, such as the stability of CO_2 or the underestimation of the O_3 and CO abundances by chemical models. However, despite their great importance on our understanding of the Martian photochemistry, there is little observational evidence constraining their abundances and variations.

In this study, we analyse 200 infrared solar occultation measurements from the ACS aboard the ExoMars TGO made during the second half of MY36 ($L_S = 212°$) and the beginning of MY37 ($L_S = 63°$) to search for spectral signatures of HO_2. In our retrieval scheme, we first analyse spectral features of CO_2 and H_2O to derive vertical profiles of pressure, temperature, and water vapour mixing ratio. Then, we analyse a spectral range including the HO_2 absorption features to constrain the abundance of this molecule in the atmosphere of Mars.

We could not confidently identify the presence of HO_2 spectral features above the level of the noise of the instrument. We therefore calculate upper limits for its abundance. We find the lowest upper limits of 15 ppbv (5σ) at approximately 10 km, increasing exponentially with altitude (∼100 ppbv at 40 km). These results improve by approximately an order of magnitude the upper limits placed for HO_2 in the atmosphere of Mars in previous investigations using ground-based infrared spectroscopy (∼200 ppbv).

Finally, we investigate whether the upper limits derived from this study are low enough to constrain the climate model chemistry schemes by comparing them with simulated vertical profiles from the OpenMARS data base. When making this comparison, we find that approximately an order of magnitude improvement in instrument sensitivity would be required to detect and/or constrain the abundance of HO_2 from 3D models including photochemistry, and approximately two orders of magnitude would be required to monitor the spatial and seasonal variations of this species.

ACKNOWLEDGEMENTS

The ExoMars mission is a joint mission of the European Space Agency (ESA) and Roscosmos. The ACS experiment is led by the Space Research Institute (IKI) in Moscow, assisted by LATMOS in France. This work was funded by the UK Space Agency and Science and Technology Facilities Council (ST/Y000234/1, ST/X006549/1, ST/Y005929/1, ST/Y006054/1, ST/V002295/1, ST/Y005414/1), Roscosmos, the National Centre for Space Studies of France (CNES) and the Ministry of Science and Education of Russia. Science operations are funded by Roscosmos and ESA.

DATA AVAILABILITY

The data sets generated by the ExoMars TGO instruments analysed in this study are available in the ESA Planetary Science Archive (PSA) repository, https://archives.esac.esa.int/psa, following a six months prior access period, following the ESA Rules on Information, Data and Intellectual Property. The retrieved vertical profiles of pressure, temperature, and water vapour mixing ratio generated in this study are publicly available in Alday (2024).

REFERENCES

Alday J., 2024, Climatology of pressure, temperature and water vapour mixing ratio from TGO/ACS, https://ordo.open.ac.uk/articles/dataset/Climatology_of_pressure_temperature_and_water_vapour_mixing_ratio_from_TGO_ACS/26308282/1
Alday J. et al., 2019, A&A, 630, A91
Alday J. et al., 2021a, Nat. Astron., 5, 943
Alday J. et al., 2021b, J. Geophys. Res., Planets, 126, e06992
Alday J. et al., 2023, Nat. Astron., 7, 867
Aoki S. et al., 2022, J. Geophys. Res., Planets, 127, e2022JE007231

Belyaev D. A. et al., 2021, Geophys. Res. Lett., 48, e93411
Belyaev D. A. et al., 2022, J. Geophys. Res., Planets, 127, e2022JE007286
Braude A. S. et al., 2022, A&A, 658, A86
Brown M. A. J. et al., 2022, J. Geophys. Res., Planets, 127, e2022JE007346
Clancy R. T. et al., 2013, Icarus, 226, 272
Daerden F., Neary L., Viscardy S., García Muñoz A., Clancy R., Smith M., Encrenaz T., Fedorova A., 2019, Icarus, 326, 197
Daerden F. et al., 2023, J. Geophys. Res., Planets, 128, e2023JE008014
Devi V. M. et al., 2017, J. Quant. Spectrosc. Radiat. Transfer, 203, 158
Fedorova A. et al., 2023, J. Geophys. Res., Planets, 128, e2022JE007348
Gamache R. R., Farese M., Renaud C. L., 2016, J. Mol. Spectrosc., 326, 144
Gordon I. E. et al., 2022, J. Quant. Spectrosc. Radiat. Transfer, 277, 107949
Holmes J. A., Lewis S. R., Patel M. R., Lefèvre F., 2018, Icarus, 302, 308
Holmes J. A. et al., 2022, J. Geophys. Res., Planets, 127, e2022JE007203
Holmes J., Lewis S., Patel M., 2024, OpenMARS MY34-35 database, https://ordo.open.ac.uk/articles/dataset/OpenMARS_MY34-35_database/24981669, last access: 2024-05-09
Irwin P. et al., 2008, J. Quant. Spectrosc. Radiat. Transfer, 109, 1136
Knutsen E. W. et al., 2021, Icarus, 357, 114266
Korablev O. et al., 2018, Space Sci. Rev., 214, 7
Korablev O. et al., 2019, Nature, 568, 517
Lefèvre F., 2004, J. Geophys. Res., 109, E07004
Lefèvre F., Krasnopolsky V., 2017, in Haberle R. M., Clancy R. T., Forget F., Smith M. D., Zurek R. W., eds, The Atmosphere and Climate of Mars. Cambridge Univ. Press, Cambridge, p. 405, https://www.cambridge.org/core/product/identifier/9781139060172
Lefèvre F. et al., 2008, Nature, 454, 971
Lefèvre F. et al., 2021, J. Geophys. Res. Planets, 126, e06838
McElroy M. B., Donahue T. M., 1972, Science, 177, 986
Millour E. et al., 2022, 16th Europlanet Science Congress 2022, Granada, Spain, p. EPSC2022–786, https://meetingorganizer.copernicus.org/EPSC2022/EPSC2022-786.html
Montmessin F. et al., 2021, A&A, 650, A140
Newville M., Stensitzki T., Allen D. B., Ingargiola A., 2014, LMFIT: Non-Linear Least-Square Minimization and Curve-Fitting for Python, https://zenodo.org/record/11813
Olsen K. S. et al., 2021, A&A, 649, L1
Parkinson T. D., Hunten D. M., 1972, J. Atmos. Sci., 29, 1380
Rodgers C. D., 2000, Inverse Methods for Atmospheric Sounding: Theory and Practice, Vol. 2. World Scientific, Singapore, p. 81, https://www.worldscientific.com/worldscibooks/10.1142/3171
Régalia L., Cousin E., Gamache R., Vispoel B., Robert S., Thomas X., 2019, J. Quant. Spectrosc. Radiat. Transfer, 231, 126
Stevens M. H. et al., 2024, J. Geophys. Res., Planets, 129, e2023JE007982
Trokhimovskiy A. et al., 2024, Icarus, 407, 115789
Villanueva G. et al., 2013, Icarus, 223, 11

This paper has been typeset from a TEX/LATEX file prepared by the author.